Applied Physics Letters

Smart optically induced nonlinear photonic crystals for frequency conversion and control

Cite as: Appl. Phys. Lett. **116**, 051104 (2020); https://doi.org/10.1063/1.5141420
Submitted: 10 December 2019 • Accepted: 21 January 2020 • Published Online: 04 February 2020

Dawei Liu, Shan Liu, Leszek Mateusz Mazur, et al.

Applied Physics Letters ARTICLE scitation.org/journal/apl

Smart optically induced nonlinear photonic crystals for frequency conversion and control

Cite as: Appl. Phys. Lett. **116**, 051104 (2020); doi: 10.1063/1.5141420
Submitted: 10 December 2019 · Accepted: 21 January 2020 ·
Published Online: 4 February 2020

Dawei Liu,[1] Shan Liu,[1] Leszek Mateusz Mazur,[2,3] Bingxia Wang,[4] Peixiang Lu,[4] Wieslaw Krolikowski,[1,2] and Yan Sheng[1,a)]

AFFILIATIONS

[1]Laser Physics Centre, Research School of Physics, The Australian National University, Canberra ACT 2601, Australia
[2]Advanced Materials Engineering and Modelling Group, Faculty of Chemistry, Wroclaw University of Science and Technology, Wyb. Wyspianskiego 27, 50-370 Wroclaw, Poland
[3]Science Program, Texas A&M University at Qatar, Doha 23874, Qatar
[4]School of Physics and Wuhan National Laboratory for Optoelectronics, Huazhong University of Science and Technology, 430074 Wuhan, China

[a)]Electronic mail: yan.sheng@anu.edu.au

ABSTRACT

We extend the functionality of nonlinear photonic crystals by fabricating a structure combining a few individual optical transformations in second harmonic generation. In particular, we employed all-optical spontaneous polarization reversal in ferroelectrics to create nonlinear holograms with curved fork-like spatial modulation of nonlinearity for the generation of second harmonic optical vortices. The curved fork-like structure represents a combination of a standard vortex harmonic generator (fork structure) and an axicon, thereby allowing us to realize the second harmonic "perfect vortices" whose diameter remains constant independently of their topological charge.

Nonlinear photonic crystals refer to the media with a spatial modulation of the second-order nonlinearity (χ^2) in one, two, or three dimensions.[1–5] They are indispensable in advanced photonics and nonlinear optics as the modulation of χ^2 allows one to control energy exchange between interacting waves. The technique that utilizes the nonlinearity periodicity to facilitate nonlinear optical interactions is known as quasi-phase matching (QPM).[6]

The spatial modulation of nonlinearity is commonly realized in ferroelectric crystals via electric poling.[7] With the advances in fundamental research and improvement in the poling techniques making the fabrication of complex and high quality ferroelectric domain structures possible,[8,9] the spectrum of application of nonlinear photonics has been significantly enhanced and ranges from laser frequency conversion to nonlinear wavefront shaping,[10,11] nonlinear optical imaging,[12] and formation of quantum light sources.[13]

The nonlinear wavefront shaping combines the functions of frequency conversion and wavefront control into a single nonlinear photonic crystal. It enables generation and control of light at new frequencies, thereby improving stability, scalability, and conversion efficiency. Recently, the concept of nonlinear holograms has been employed to implement nonlinear wavefront shaping.[14,15] The typical example is the vortex harmonic generation using fork-like nonlinear photonic structures. Nonlinear diffraction of incident plane waves on such a structure leads to the generation of vortex beams at the second harmonic frequency.[16] In order to implement multiple operations with a single crystal, Liu *et al.*[17] employed the femtosecond laser poling technique to inscribe various ferroelectric domain structures in different depths of the crystal, such that the second harmonics with spiral, conical, and Gaussian wavefront shapes were obtained simultaneously. Later on, Wei *et al.*[18] fabricated multiple layers of fork-like domain structures, in which the periodicity along the longitudinal direction ensures the fulfillment of phase matching conditions to increase the conversion efficiency of nonlinear wavefront shaping.

The nonlinear hologram has been proved to be an efficient method for the realization of nonlinear wavefront shaping. In contrast to its linear analog, however, the study on the nonlinear hologram is still very limited, and only the simplest case was realized, i.e., using the interference pattern to generate optical beams at a frequency different from the incident wave, having simultaneously its wavefront spatially shaped [Fig. 1(a)]. More complex shape control and manipulations typically require the generated signal from the nonlinear photonic

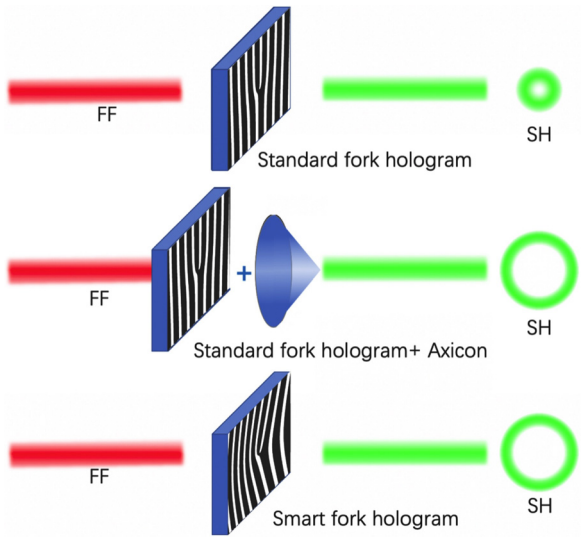

FIG. 1. Illustrating the concept of extended functionalities of nonlinear photonic crystals (NPC). (a) Traditional NPC-nonlinearity pattern (here fork hologram) results in the emission of the second harmonic signal in the form of a standard optical vortex. (b) Combined action of the NPC and an external axicon leads to the formation of perfect vortex harmonic. (c) The smart NPC with nonlinearity modulation representing the combined action of the fork pattern and axicon, resulting in the generation of a perfect vortex at the second harmonic frequency.

crystal to be further processed by additional optical components such as lenses or axicons [Fig. 1(b)].

In this work, we show that in fact we can integrate functions of many optical components into a single nonlinear photonic crystal, which makes the complex control of the nonlinear optical interactions possible. As a specific case, we combined the nonlinear fork structure with an axicon, and instead of a standard vortex second harmonic beam, here we observed the perfect vortex second harmonic, whose diameters do not change with the topological charge [Fig. 1(c)]. While the perfect vortex beam has been realized recently in linear optics,[19,20] it has never been demonstrated in the nonlinear regime.

The essential element of nonlinear wave shaping is a nonlinear hologram or a nonlinear photonic crystal, i.e., a nonlinear medium with a uniform refractive index but spatially modulated nonlinearity, which in our case has a form of curved fork grating. The curved fork pattern was designed following the prescription in Ref. 20. We assumed the refractive index of the axicon as $n = 1.48$ and the wavelength of interfering conical and singular waves as $\lambda = 1250$ nm. To achieve the spatial nonlinearity modulation, we employed our all-optical domain reversal technique.[8] We fabricated the nonlinearity structure in a Z-cut 500 μm thick, as-grown, sample of ferroelectric Calcium Barium Niobate (CBN). The femtosecond laser beam at 800 nm from the Coherent Mira 900 laser passed through the shutter and was subsequently tightly focused inside the CBN sample by a 50× microscope objective (NA = 0.65). The sample was mounted on the computer-controlled XYZ translation stage. The domain reversal process involved the following steps: First the shutter was open for 0.1 s, during which the sample was translated (with a speed of 2500 micrometers/s) along the Z-axis. During this stage, the nonlinear absorption of the light beam in the focal volume caused local heating of the crystal. This resulted in the appearance of a thermal electric field whose strength exceeded the coercive field of the crystal (here 1 kV/cm), leading to local reversal of spontaneous polarization. The Z-translation of the focal region resulted in the formation of some 50 μm long ferroelectric domain in the sample. After the shutter had been closed, the sample was translated in the X-Y plane to a neighboring location. Then, the shutter was opened letting the beam in, and the sample's translation along the Z-axis followed. Repeating the procedure many times resulted in the creation of macroscopic-size nonlinearity patterns consisting of elongated single ferroelectric domains. The final domain pattern covered an area of roughly 60 μm × 60 μm. The fabricated domain structures were visualized by using nonlinear Čerenkov microscopy.[12] In Fig. 2, we depict a few examples of the fork structures for different values of topological charge (l) and the conical parameter (γ). The point-like internal structure of the patterns reflecting the writing process is clearly visible. It is worth noting that the images represent the ferroelectric domain structure and not the refractive index, which is basically unaffected by the laser writing process.

The fabricated curved fork structures were subsequently used in second harmonic generation experiments. As a light source, we used a Chameleon Ultra II (Coherent) that was pumping synchronous Compact OPO (Coherent) with a train of 130 fs pulses with a repetition rate of 80 MHz. The linearly polarized fundamental beam was loosely focused (using a microscopic objective 10×, NA = 0.1) in the fork region. The typical input power was 350 mW. The nonlinear diffraction in the structure led to the emission of the second harmonic waves in multiple diffraction orders. We recorded the spatial intensity distribution of the strongest, the first diffraction order using a CCD camera.

Even though the nonlinearity patterns were thin (50 micrometers), they provided enough propagation distance for the FF beam

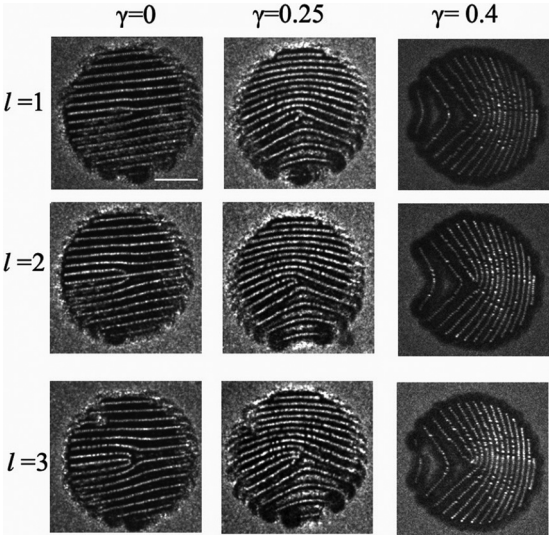

FIG. 2. Nonlinear microscopic images of the curved fork nonlinearity structures fabricated via the all-optical domain reversal in the ferroelectric CBN crystal. 2D images of the nonlinearity pattern for three values of topological charge ($l = 1$, 2, and 3) and conical parameter, $\gamma = 0.0$, 0.25, and 0.4, respectively. The scale bar in the top left graph corresponds to 20 μm.

to obtain the desired spatial structure of the second harmonic beam. Typical experimental results are depicted in Fig. 3. The pictures show the intensity distribution of the second harmonic beam as a function of the topological charge and axicon angle. One can see that the diameter of vortices generated from the fork patterns with the increasing value of the conical parameter is almost constant for the varying topological charge. This is better visualized in the graph in Fig. 4, which depicts the measured diameter of the vortex (normalized to its value for charge $l = 1$) as a function of topological charge. Already, for small conicity ($\gamma = 0.1$), the vortex diameter varies very weakly with the charge. For $\gamma \geq 0.25$, these ring beams maintain almost a constant diameter, irrespective of the charge. This actually represents the nonlinearly generated perfect vortices.

The experimental images in Fig. 3 show partially closed vortex rings for $\gamma = 0.25$ and higher. This effect is caused by the small area of our fabricated structures. For large γ, there is not enough fringes within the area illuminated by a fundamental beam to generate a complete vortex beam. This is clearly visible in Fig. 2, for $\gamma = 0.4$. To remedy this, the fabricated structure must have a greater spatial dimension, so the complete phase structure of the vortex beam can be restored in the frequency conversion process. Furthermore, there is a visible noise signal to the right of the generated vortices. The noise is brought about by strong conical (Čerenkov) emission of second harmonic caused by the random ferroelectric domains present in our as-grown crystal. The electrical poling of the whole sample would remove those random domains and eliminate the noise.

In addition, the experimental results (see Fig. 3) show that the structure with $\gamma = 0.25$ gives rise to stronger SHG compared with the other samples. In order to comprehend this phenomenon, we simulate the generation of second harmonic vortices from curved fork structures, using the split-step Fast Fourier Transform-based beam propagation method. Because of low conversion efficiency, we assumed

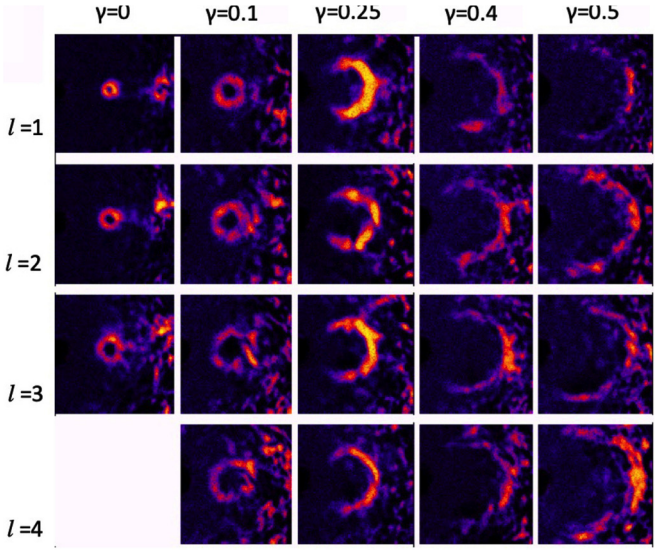

FIG. 3. Spatial intensity distribution of the emitted second harmonic beam after the illumination of nonlinear holograms with a 1250 nm femtosecond fundamental beam. Each image represents the generated second harmonic vortex beam for a particular value of conical parameter γ and topological charge l.

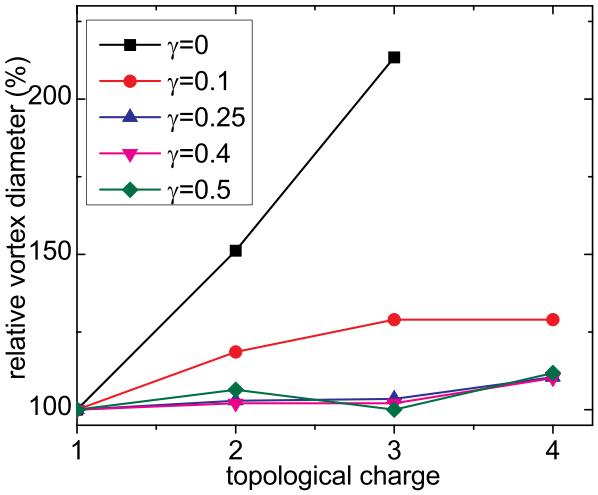

FIG. 4. Relative diameter of the generated vortex beam as a function of topological charge (l) and conical parameter γ.

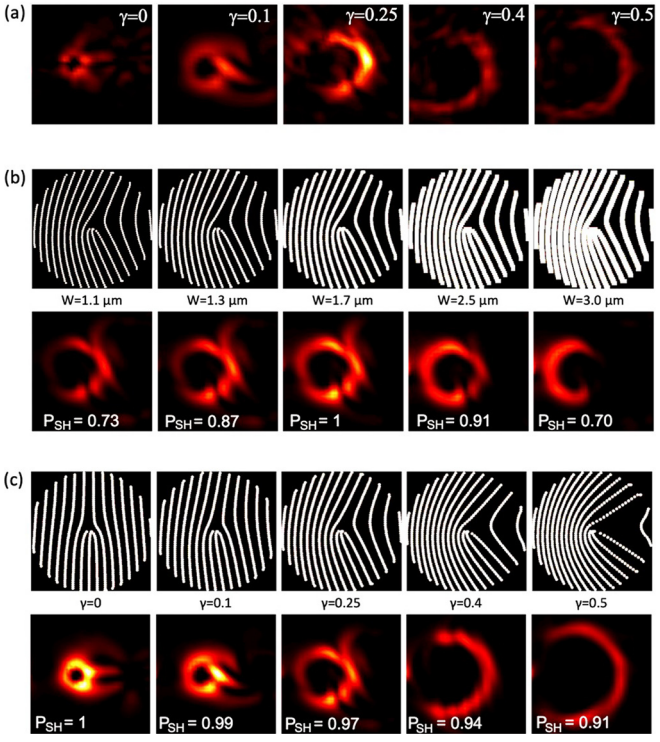

FIG. 5. Simulations of the vortex second harmonic generation from the fork-shaped, 60 μm × 60μm wide, nonlinear photonic crystals. (a) The calculated SH generated from samples with different values of γ and widths of inverted ferroelectric domains. The patterns of the real fabricated samples are used in these simulations. (b) The dependence of the vortex second harmonic on the width of the inverted domains (w) for a fixed value of $\gamma = 0.25$. (c) The influence of conical parameter γ on the vortex second harmonic generation with the width of the inverted domains of 1.7 μm.

undepleted propagation of the fundamental beam through the fork-shaped nonlinear photonic crystal. We use the dispersion data of the CBN crystal.[21] Simulation results are summarized in Fig. 5. In particular, graphs in Fig. 5(a) represent the calculated SH vortex by using the real experimentally fabricated nonlinearity patterns. It is seen that, in agreement with the experiment, the vortex at $\gamma = 0.25$ is clearly stronger than those obtained for other values of the conical parameter.

A further analysis of dependence of the strength of second harmonic on different structural parameters included the role of the duty cycle, i.e., the ratio of the area of inverted ferroelectric domains to that of the whole sample. It is well known that varying the duty cycle one can control the strength of emitted SH.[3] In the top row of Fig. 5(b), we depict the curved nonlinearity pattern with $\gamma = 0.25$ and charge $l = 3$, realized with different widths (w) of the inverted domains. The bottom row of Fig. 5(b) shows the emitted second harmonic beam generated by each corresponding structure with numbers indicating the relative power of the SH beam. The presence of an optimum linewidth (and subsequently the duty cycle) is evident. While much efforts have been made to fabricate the same-quality curved fork structures, varying only the value of conical parameter γ, it turned out the linewidth in the sample with $\gamma = 0.25$ was slightly larger and at the same time closer to the optimum value than in others structures.

Finally, in Fig. 5(c), we also show the predicted vortex SHG assuming all the samples with different γ values having the same duty cycle determined by the inverted domain linewidth $w = 1.7\mu$m. It is clear that the variation of γ have very little effect on the strength of the emitted SH vortex beam, except for large γ like $\gamma = 0.4$ and 0.5, when the strength of the second harmonic decreases due to the vanishing of the part of the SH circles (Fig. 3).

In conclusion, we have fabricated curved fork spatial nonlinearity patterns in a calcium barium niobate crystal using laser-induced ferroelectric domain inversion. The 50 micrometer thick structures were employed as nonlinear holograms generating second harmonic beams in the form of optical vortices. By imposing a conical angle onto the fork structures, we were able to achieve the insensitivity of the radius of generated vortices on the topological charge. This result, which constitutes the experimental observation of the so-called perfect vortices via the nonlinear beam shaping, represents at the same time the extension of functionalities of nonlinear photonic crystals.

This work was supported by the Qatar National Research Fund (Grant No. NPRP 12S-0205-190047) and Australian Research Council.

REFERENCES

[1]V. Berger, Phys. Rev. Lett. **81**, 4136 (1998).
[2]N. G. R. Broderick, G. W. Ross, H. L. Offerhaus, D. J. Richardson, and D. C. Hanna, Phys. Rev. Lett. **84**, 4345 (2000).
[3]A. Arie and N. Voloch, Laser Photonics Rev. **4**, 355 (2010).
[4]T. Xu, K. Switkowski, X. Chen, S. Liu, K. Koynov, H. Yu, H. Zhang, J. Wang, Y. Sheng, and W. Krolikowski, Nat. Photonics **12**, 591 (2018).
[5]D. Wei, C. Wang, H. Wang, X. Hu, D. Wei, X. Fang, Y. Zhang, D. Wu, Y. Hu, J. Li *et al.*, Nat. Photonics **12**, 596 (2018).
[6]J. A. Armstrong, N. Bloembergen, J. Ducuing, and P. S. Pershan, Phys. Rev. **127**, 1918 (1962).
[7]M. Yamada, N. Nada, and M. Saitoh, Appl. Phys. Lett. **62**, 435 (1993).
[8]X. Chen, P. Karpinski, V. Shvedov, K. Koynov, B. Wang, J. Trull, C. Cojocaru, Y. Sheng, and W. Krolikowski, Appl. Phys. Lett. **107**, 141102 (2015).
[9]C. Y. J. Ying, A. C. Muir, C. E. Valdivia, H. Steigerwald, C. L. Sones, R. W. Eason, E. Soergel, and S. Mailis, Laser Photonics Rev. **6**, 526 (2012).
[10]T. Ellenbogen, N. Voloch-Bloch, A. Ganay-Padowicz, and A. Arie, Nat. Photonics **3**, 395 (2009).
[11]X. P. Hu, Y. Zhang, and S. N. Zhu, Adv. Mater. **31**, 1903375 (2019).
[12]Y. Sheng, A. Best, H. Butt, W. Krolikowski, and K. Koynov, Opt. Express **18**, 16539 (2010).
[13]H. Jin, F. M. Liu, P. Xu, J. L. Xia, M. L. Zhong, Y. Yuan, J. W. Zhou, Y. X. Gong, W. Wang, and S. N. Zhu, Phys. Rev. Lett. **113**, 103601 (2014).
[14]A. Shapira, I. Juwiler, and A. Arie, Opt. Lett. **36**, 3015 (2011).
[15]X. Hong, B. Yang, C. Zhang, Y. Qin, and Y. Zhu, Phys. Rev. Lett. **113**, 163902 (2014).
[16]N. V. Bloch, K. Shemer, A. Shapira, R. Shiloh, I. Juwiler, and A. Arie, Phys. Rev. Lett. **108**, 233902 (2012).
[17]S. Liu, K. Switkowski, C. Xu, J. Tian, B. Wang, P. Lu, W. Krolikowski, and Y. Sheng, Nat. Commun. **10**, 3208 (2019).
[18]D. Wei, C. Wang, X. Xu, H. Wang, Y. Hu, P. Chen, J. Li, Y. Zhu, C. Xin, X. Hu *et al.*, Nat. Commun. **10**, 4193 (2019).
[19]A. S. Ostrovsky, C. Rickenstorff-Parrao, and V. Arrizón, Opt. Lett. **38**, 534 (2013).
[20]S. Topuzoski, Opt. Quantum Electron. **48**, 138 (2016).
[21]M. Eβer, M. Burianek, P. Held, J. Stade, S. Bulut, C. Wickleder, and M. Mühlberg, Cryst. Res. Technol. **38**, 457 (2003).